Article

J. Biol. Regul. Homeost. Agents. 2024; 38(5): 3945–3959
https://doi.org/10.23812/j.biol.regul.homeost.agents.20243805.312

Knockdown of Opsin 3 (OPN3) Enhances G6PD Autophagic Degradation and Aggravates Oxidative Stress Damage to Radiosensitize Cervical Cancer Cells

Yanyan Li[1], Xiaodong Wang[2,*]

[1]Postpartum Pelvic Floor Rehabilitation Clinic, Yantaishan Hospital, 264003 Yantai, Shandong, China
[2]Radiotherapy Department I, Yantaishan Hospital, 264003 Yantai, Shandong, China
*Correspondence: 18953541288@163.com (Xiaodong Wang)
Published: 1 May 2024

Background: Cervical cancer (CC) is the fourth most prevalent cancer among women worldwide, imposing a significant burden. While radiotherapy is a cornerstone in CC treatment, radioresistance remains a challenge, necessitating the exploration of mechanisms and novel targets for overcoming this challenge. Opsin 3 (*OPN3*) has been implicated in cancer treatment resistance, and the glucose-6-phosphate dehydrogenase (*G6PD*)-mediated glucose metabolism, along with oxidative stress, has been associated with radioresistance. This study aimed to explore the impact of *OPN3* knockdown on the radioresistance of CC cells and the involvement of *G6PD* and oxidative stress in the underlying mechanisms.

Methods: The HeLa cell line, a representative of CC, was utilized in this study. *OPN3* knockdown was established through cell transfection. The subsequent effects on HeLa cell viability and apoptosis under ionizing radiation (IR) were assessed using cell counting kit-8 (CCK-8) assay, colony forming assay, terminal deoxynucleotidyl transferase (TdT) dUTP nick-end labeling (TUNEL) assay, and western blot analysis to detect apoptosis-related proteins. Additionally, proteins associated with oxidative stress, DNA damage, and G6PD protein levels and activity were measured using enzyme-linked immunosorbent assay (ELISA) and western blot. Acquired radioresistant HeLa cells (RR-HeLa) were generated using IR. *OPN3* knockdown was performed in RR-HeLa cells, and subsequent effects were assessed as described for HeLa cells. Reactive oxygen species (ROS) scavenger and *G6PD* inhibitor were employed to investigate the role of *OPN3* in regulating oxidative stress and *G6PD* during radioresistance. Furthermore, in the *G6PD* degradation, autophagy inhibitor and proteasome pathway inhibitor were used to confirm the regulatory role of *OPN3* on *G6PD* through autophagy.

Results: *OPN3* was upregulated in RR-HeLa cells ($p < 0.001$). *OPN3* knockdown decreased the proliferation ($p < 0.001$), DNA damage ($p < 0.001$), and oxidative stress ($p < 0.001$) while reducing cell apoptosis ($p < 0.001$), glucose metabolism ($p < 0.001$), G6PD protein levels ($p < 0.001$), and activity ($p < 0.001$) in HeLa and RR-HeLa cells following IR treatment. *OPN3* overexpression in HeLa cells increased proliferation post-IR treatment. The post-IR cell proliferation reduction induced by *OPN3* knockdown was reversed by ROS inhibitor and G6PD overexpression ($p < 0.001$), while further decreased by *G6PD* inhibitor ($p < 0.001$). The *OPN3* knockdown-induced decrease in G6PD was unchanged by the proteasome pathway inhibitor ($p > 0.05$) but was reversed by the autophagy inhibitor ($p < 0.001$), thereby reversing the post-IR cell proliferation ($p < 0.001$).

Conclusion: *OPN3* knockdown renders HeLa cells more radiosensitive and mitigates radioresistance by promoting the autophagic degradation of G6PD and exacerbating oxidative stress within the cells.

Keywords: opsin 3; cervical cancer; *G6PD*; oxidative stress; autophagic degradation

Introduction

Cervical cancer (CC), according to the 2020 global estimates, is the fourth most prevalent cancer and the fourth leading cause of cancer-related deaths in women worldwide [1]. Reports indicate that the CC contributes to 8% of all cancer-related female deaths annually [2]. The predominant histological types of CC include adenocarcinoma, comprising 20%, and squamous cell carcinoma, comprising 80% [3,4]. Mostly, CC affects women under 50 years old [5], and there were approximately 570,000 new cases of CC in 2018 [6,7]. Moreover, in the United States alone, there were 14,000 newly diagnosed CC cases, resulting in 4000 deaths annually [8]. Nearly 84% of CC cases and 88% of CC-related deaths occur in low- and middle-income countries [9]. However, populations with high incidence rates of CC and poor outcomes persist even in countries with adequate resources [10]. Given the significant portion of the global cancer burden attributed to CC, there is an urgent need for novel and effective treatments or the optimization of existing therapies to ameliorate CC and enhance the quality of life for CC patients.

Journal of
BIOLOGICAL REGULATORS
and Homeostatic Agents

Key treatments for CC include surgery, chemotherapy, radiotherapy (RT), and immunotherapy, with external beam radiation therapy and brachytherapy playing significant roles [11,12]. As the primary treatment strategy for locally advanced CC (LACC), RT induces direct DNA damage in tumor cells by causing DNA double-strand breaks (DSBs) or indirectly by generating reactive oxygen species (ROS), subsequently leading to DNA damage [13–15]. However, despite the advancements in RT efficacy for CC patients, the emergence of radioresistance remains a major challenge [16,17]. Therefore, there is a critical need to investigate the mechanism underlying radioresistance to overcome this challenge and enhance the efficacy of RT in CC treatment.

Opsin 3 (*OPN3*), known as encephalopsin, has been proved to be functionally linked to tumorigenesis, clinical prognosis, and treatment resistance across various cancers [18–20]. However, the precise functions of *OPN3* in human cancers, primarily its impact on the radioresistance in RT for CC, remain elusive. Furthermore, the glucose metabolism, encompassing oxidative phosphorylation, glycolysis, and the pentose phosphate pathway (PPP), is closely associated with radioresistance [21]. Notably, the glucose-6-phosphate dehydrogenase (*G6PD*) is a pivotal enzyme regulating the rate of the PPP and its substrate, glucose-6-phosphate, links glycolysis with the PPP [22]. Moreover, enhanced G6PD autophagic degradation has been demonstrated to lead to radiosensitivity in small-cell lung cancer cells [23].

Given that HeLa cells exhibit robust radioresistance compared to other cancer cell lines, this study aimed to explore the influence of *OPN3* on radioresistance in HeLa CC cells and elucidate the underlying mechanisms involving G6PD degradation and oxidative stress [24]. This study contributes to a deeper understanding of the role of *OPN3* in cancers and treatment resistance and identifies potential targets for optimizing therapeutic strategies in RT for CC.

Materials and Methods

Cell Culture and Reagent Treatments

The human CC cell line HeLa (iCell-h088) was procured from iCell Bioscience Inc. (Shanghai, China) and cultured in the specific medium for HeLa (iCell-h088-001b, iCell Bioscience Inc., Shanghai, China) under standard conditions of 37 °C, 70–80% humidity, and 5% CO_2. When inhibition of ROS in HeLa cells was necessary, N-acetylcysteine (NAC; HY-B0215, MedChemExpress, Monmouth Junction, NJ, USA) was supplemented into the culture medium (3 nM [25]). For inhibition of *G6PD* in HeLa cells, the 6-aminonicotinamide (6-AN; HY-W010342, MedChemExpress, Monmouth Junction, NJ, USA) was added to the culture medium (100 nM [26]). Autophagy in HeLa cells was suppressed by adding the autophagy inhibitor chloroquine (an autophagy inhibitor) (CQ; HY-17589A, MedChemExpress, Monmouth Junction, NJ, USA) to the culture medium (20 μM [27]), while the ubiquitin-proteasome pathway was inhibited by supplementing the medium with the inhibitor Z-Leu-Leu-Leu-al (MG132; HY-13259, MedChemExpress, Monmouth Junction, NJ, USA) at a concentration of 10 μM [28]. Prior to experimental use, cells were authenticated using short tandem repeat (STR), and mycoplasma contamination was routinely monitored and addressed to ensure cell line integrity.

Ionizing Radiation (IR)

HeLa cells were seeded and allowed to attach overnight. Irradiation was performed using the small animal radiation research platform (SARRP; Xstrahl Inc., Suwanee, GA, USA). To establish radioresistant HeLa cells, cells were first allowed to adhere to the wall of the culture flask, followed by a single dose of 2-Gy irradiation. Subsequently, cells were cultured and closely monitored. Upon cellular recovery, a subsequent 2-Gy dose of irradiation was administered. The above procedures were repeated until a total dose of 60 Gy (30 doses of 2-Gy each) was delivered. Surviving HeLa cells were considered as the established radioresistant HeLa cells (RR-HeLa) [23].

Cell Transfection

For *OPN3* knockdown in HeLa cells, small interfering RNA (siRNA) targeting *OPN3* (si-*OPN3*; 5′-CCUGGUCACUCCAACAAUATT-3′) or negative control scramble siRNA (*si-NC*; 5′-UUCUCCGAACGUGUCACGUTT-3′) was obtained from GenePharma (Shanghai, China) and transfected into HeLa cells using the Silencer™ siRNA transfection kit (AM1631, Invitrogen, Carlsbad, CA, USA) following the manufacturer's instructions. Lentiviruses containing the pSIN-EF2 vector carrying full-length of *OPN3* (OE-*OPN3*; Gene ID: 1122) or *G6PD*-overexpressing plasmids (OE-*G6PD*; Gene ID: 8517) and the empty vector (OE-NC), were purchased from GeneChem (Shanghai, China) and transfected into HeLa cells when the cell density reached 9 $\times$ 10^4 cells/dish, following the manufacturer's instructions. Transfection efficiency was assessed by RT-qPCR and/or western blot analysis after 72 hours of incubation.

Cell Counting Kit-8 (CCK-8) Assays

Following exposure to ionizing radiation (IR) or control conditions, the cell proliferation was measured after 72 hours of culture. Cells were washed with phosphate-buffered saline (PBS; C0221A, Beyotime, Shanghai, China) and incubated in fresh culture medium supplemented with 10 μL of CCK-8 solution (C0037, Beyotime, Shanghai, China) for 4 hours at 37 °C. Subsequently, the optical density (OD) at 450 nm was measured using a microplate reader (Multiskan Sky, ThermoFisher Scientific, Shanghai, China).

Colony Formation Assay

Cells (1×10^5 cells/well) were seeded in 6-well plates. After exposure to IR or control conditions, cells were cultured for 72 hours. After removing any supplemented chemical reagents, cells were normally cultured for an additional 10 days. Subsequently, cells were fixed with 4% paraformaldehyde (P0099, Beyotime, Shanghai, China) for 15 minutes and stained with 0.5 crystal violet (C0121, Beyotime, Shanghai, China) for 15 minutes. The formed colonies were visualized and captured under a microscope (CKX53, Olympus, Tokyo, Japan). Colony counting was performed using ImageJ software (version 1.48, National Institutes of Health, Bethesda, MD, USA), and colonies with more than 50 cells were considered for calculating the survival fraction.

Terminal Deoxynucleotidyl Transferase (TdT) dUTP Nick-End Labeling (TUNEL) Assay

Following exposure to IR or control conditions, cells were cultured with the designated treatments for 48 hours. Subsequently, cells were washed with PBS and fixed with 4% paraformaldehyde (P0099, Beyotime, Shanghai, China) for 30 minutes, followed by permeabilization using a permeabilization solution (P0097, Beyotime, Shanghai, China). In a dark environment, cells were incubated with 50 µL of TUNEL reagent (C1088, Beyotime, Shanghai, China) for 60 minutes at 37 °C. After washing with PBS, cells were stained with 2-(4-Amidinophenyl)-6-indolecarbamidine dihydrochloride (DAPI; C1002, Beyotime, Shanghai, China), and TUNEL-positive cells were visualized under a microscope (CKX53, Olympus, Tokyo, Japan). The rate of cell apoptosis was calculated by randomly selecting three or more fields and applying the following formula: Cell apoptosis rate = 100% × (number of apoptotic cells [green])/(total number of cells [blue]).

RT-qPCR

Following exposure to IR or control conditions, cells were cultured with the designated treatments for 24 hours. Subsequently, total RNA was extracted from cells using TRIzol reagent (R0016, Beyotime, Shanghai, China). A 3 µL aliquot of the RNA sample was utilized for cDNA synthesis with the FastQuant cDNA (KR116, Tiangen, Beijing, China). The qPCR reaction was performed using the BeyoFast™ SYBR Green One-Step qRT-PCR kit (D7268S, Beyotime, Shanghai, China) in the PCR instrument (LightCycler96, Roche, Shanghai, China). Expression levels were determined using the $2^{-\Delta\Delta Ct}$ method, with glyceraldehyde-3-phosphate dehydrogenase (*GAPDH*) as the internal reference. Primer sequences used are listed in Table 1.

Table 1. Primer sequences used in this study.

Name	Sequence (5′-3′)
OPN3-F	CAATCCAGTGATTTATGTCTTCATGATCAGAAAG
OPN3-R	GCATTTCACTTCCAGCTGCTGGTAGGT
GAPDH-F	GACATCCGCAAAGACCTG
GAPDH-R	GGAAGGTGGACAGCGAG

OPN3, opsin 3; *GAPDH*, glyceraldehyde-3-phosphate dehydrogenase; F, forward; R, reverse.

Western Blot Analysis

Following exposure to IR or control conditions, cells were cultured with the designated treatments for 24 hours. Subsequently, total proteins were extracted from cells using radioimmunoprecipitation assay (RIPA) lysis buffer containing phenylmethylsulfonyl fluoride (PMSF) (R0010, Solarbio, Beijing, China). For western blot analysis, 40 µg of protein was separated by sodium dodecyl sulfate-polyacrylamide gel electrophoresis (SDS-PAGE; 10%; P0012A, Beyotime, Shanghai, China). The separated proteins were then transferred onto nitrocellulose membranes (IPVH00010, Millipore, Billerica, MA, USA). After blocking with 5% nonfat milk for 2 hours at room temperature, the membranes were incubated with primary antibodies overnight at 4 °C, followed by incubation with secondary antibodies for 2 hours. Primary antibodies used were anti-*OPN3* (1:1000 dilution; PA5-106831, Invitrogen, Carlsbad, CA, USA), anti-poly (ADP-ribose) polymerase 1 (anti-PARP1; 1:1000 dilution; ab191217, Abcam, Cambridge, MA, USA), anti-cleaved-PARP1 (1:1000 dilution; ab32064, Abcam, Cambridge, MA, USA), anti-nuclear factor erythroid 2-related factor 2 (anti-Nrf2; 1:1000 dilution; ab137550, Abcam, Cambridge, MA, USA), anti-phosphorylated Nrf2 (anti-p-Nrf2; 1:1000 dilution; PA5-67520, Invitrogen, Carlsbad, CA, USA), anti-G6PD (1:1000 dilution; ab133525, Abcam, Cambridge, MA, USA), anti-light chain 3B (anti-LC3B; 1:1000 dilution; ab48394, Abcam, Cambridge, MA, USA), and anti-GAPDH (1:1000 dilution; ab8245, Abcam, Cambridge, MA, USA). The Rabbit anti-Human IgG Fc Secondary antibody (1:10000 dilution; 31423, Invitrogen, Carlsbad, CA, USA) was used as the secondary antibody for 2 hours. Protein bands were visualized using an Enhanced chemiluminescence (ECL) kit (P0018S, Beyotime, Shanghai, China), and grayscale values were analyzed using ImageJ software (version 1.48, National Institutes of Health, Bethesda, MD, USA).

Enzyme-Linked Immunosorbent Assay (ELISA)

Following exposure to IR or control conditions, cells were cultured with the designated treatments for 24 hours. Subsequently, the levels of the following components in cells were measured following manufacturers' instructions: gamma histone 2AX (γ-H2AX; ab279817, Abcam, Cambridge, MA, USA), dihydronicotinamide adenine dinucleotide phosphate (NADPH; S0179, Beyotime, Shanghai, China), ROS (S0033S, Beyotime, Shanghai, China), lactic acid (D799851, Sangon Biotech Co., Shanghai, China),

Journal of
BIOLOGICAL REGULATORS
and Homeostatic Agents

glucose transporter type 1 (GLUT1; E-EL-H1822c, Elabscience Biotechnology Co., Ltd., Wuhan, China), G6PD (E-EL-H1816c, Elabscience Biotechnology Co., Ltd., Wuhan, China), and G6PD activity (ab176722, Abcam, Cambridge, MA, USA). Each measurement was performed using ELISA kits specific to the respective targets.

Statistical Analysis

Data were analyzed using GraphPad Prism software (version 8.0.2, La Jolla, CA, USA) and were expressed as mean ± standard deviation. One-way analysis of variance (ANOVA) followed by Turkey's post hoc test was used for comparisons among multiple groups, while student's *t*-test was employed for pairwise comparisons. A significance level of $p < 0.05$ was considered statistically significant.

Results

Downregulation of OPN3 Enhances Radiosensitivity in HeLa Cells

We initially verified the efficacy of siRNA transfection. As illustrated, *OPN3* protein (Fig. 1A; $p < 0.001$) and mRNA (Fig. 1B; $p < 0.001$) were significantly downregulated in si-*OPN3* transfected HeLa cells (HeLa+si-*OPN3*) compared to si-NC transfected HeLa cells (HeLa+si-NC), confirming successful transfection and *OPN3* knockdown. Moreover, 24 hours after exposure to 2-Gy IR, the downregulation of *OPN3* protein ($p < 0.001$) and mRNA ($p < 0.001$) persisted in HeLa+si-*OPN3* compared to HeLa+si-NC. Additionally, after IR treatment, the *OPN3* mRNA and protein levels increased in HeLa and HeLa+si-NC cells ($p < 0.05$). Following exposure to 2-Gy IR, the CCK-8 assay was employed to measure cell proliferation (Fig. 1C). The results demonstrated that IR impaired HeLa cell proliferation ($p < 0.01$), which was further reduced in HeLa+si-*OPN3* cells ($p < 0.001$). Similarly, in Fig. 1D, 72 hours post-exposure to 2-Gy IR, the survival fraction of HeLa+si-*OPN3* was significantly lower compared to that of HeLa+si-NC cells ($p < 0.05$), indicating increased vulnerability to IR in HeLa+si-OPN3 cells.

The results of the TUNEL assay (Fig. 1E) revealed that 2-Gy IR induced apoptosis in HeLa cells ($p < 0.001$), with a further increase observed in HeLa+si-*OPN3* cells compared to HeLa+si-NC cells ($p < 0.001$). These findings were verified by the western blot results in Fig. 1F, showing that after the 2-Gy IR treatment, Cleaved-PARP1/PARP1 levels increased in HeLa cells ($p < 0.05$), with a further elevation observed in HeLa+si-*OPN3* cells compared to HeLa+si-NC cells ($p < 0.001$). Taken together, these findings suggest that the *OPN3*-knockdown HeLa cells exhibit increased radiosensitivity and are more susceptible to cell death induced by IR.

OPN3 Knockdown Increases DNA Damage and Oxidative Stress Induced by IR

As the molecular marker of DNA damage, γ-H2AX levels were elevated in HeLa cells following IR treatment (Fig. 2A; $p < 0.001$). Moreover, compared to HeLa+si-NC cells, HeLa+si-*OPN3* cells exhibited significantly higher levels of γ-H2AX in response to IR ($p < 0.001$), indicating more severe DNA damage in *OPN3*-knockdown HeLa cells. Moreover, Nrf2 is an antioxidant protein that protects cells from oxidative stress and phosphorylated Nrf2 (p-Nrf2) accumulates under oxidative stress conditions [29]. As shown in Fig. 2B, levels of p-Nrf2/Nrf2 increased in HeLa cells following IR treatment ($p < 0.001$), with a further elevation observed in HeLa+si-*OPN3* cells compared to HeLa+si-NC cells ($p < 0.001$).

Additionally, IR induced a decrease in NADPH levels (Fig. 2C; $p < 0.01$) and an increase in ROS levels (Fig. 2D; $p < 0.001$) in HeLa cells. Furthermore, HeLa+si-*OPN3* cells treated with IR exhibited lower NADPH levels ($p < 0.001$) and higher ROS levels ($p < 0.001$) compared to Hela+si-NC cells treated with IR. These findings suggest that the IR induces DNA damage and oxidative stress in HeLa cells, and these effects are exacerbated when *OPN3* is knocked down.

OPN3 Knockdown Suppresses G6PD-Mediated Glucose Metabolism

We further investigated whether *OPN3*-regulated radioresistance was associated with glucose metabolism and G6PD. As shown in Fig. 2E, lactic acid production was significantly reduced in si-*OPN3* transfected HeLa cells compared to si-NC transfected HeLa cells ($p < 0.001$). Moreover, the level of GLUT1 was decreased in HeLa cells following IR treatment (Fig. 2F; $p < 0.05$), with a further reduction observed in si-*OPN3* transfected HeLa cells (Fig. 2F; $p < 0.001$). These findings indicate that IR-induced suppression of glucose metabolism is enhanced in *OPN3*-knockdown HeLa cells compared to HeLa cells.

Additionally, we observed that the alteration in glucose metabolism was associated with G6PD activity, as IR treatment led to a decrease in G6PD activity in HeLa cells (Fig. 2G; $p < 0.05$), which was further reduced in *OPN3*-knockdown HeLa cells (Fig. 2G; $p < 0.01$). These findings suggest that the effect of *OPN3* on glucose metabolism may be associated with promoting G6PD degradation.

Successful Establishment of Acquired Radioresistant HeLa Cells with Different OPN3 Expression Levels

We established the acquired radioresistant HeLa cells (RR-HeLa) by exposing HeLa cells to X-rays at a dose of 2 Gyper treatment, repeated for a total of 60 Gy. The western blot results (Fig. 3) demonstrated that *OPN3* levels were increased in RR-HeLa cells compared to HeLa cells ($p < 0.001$). Additionally, *OPN3* protein levels were decreased in RR-HeLa+si-*OPN3* cells compared to RR-HeLa cells

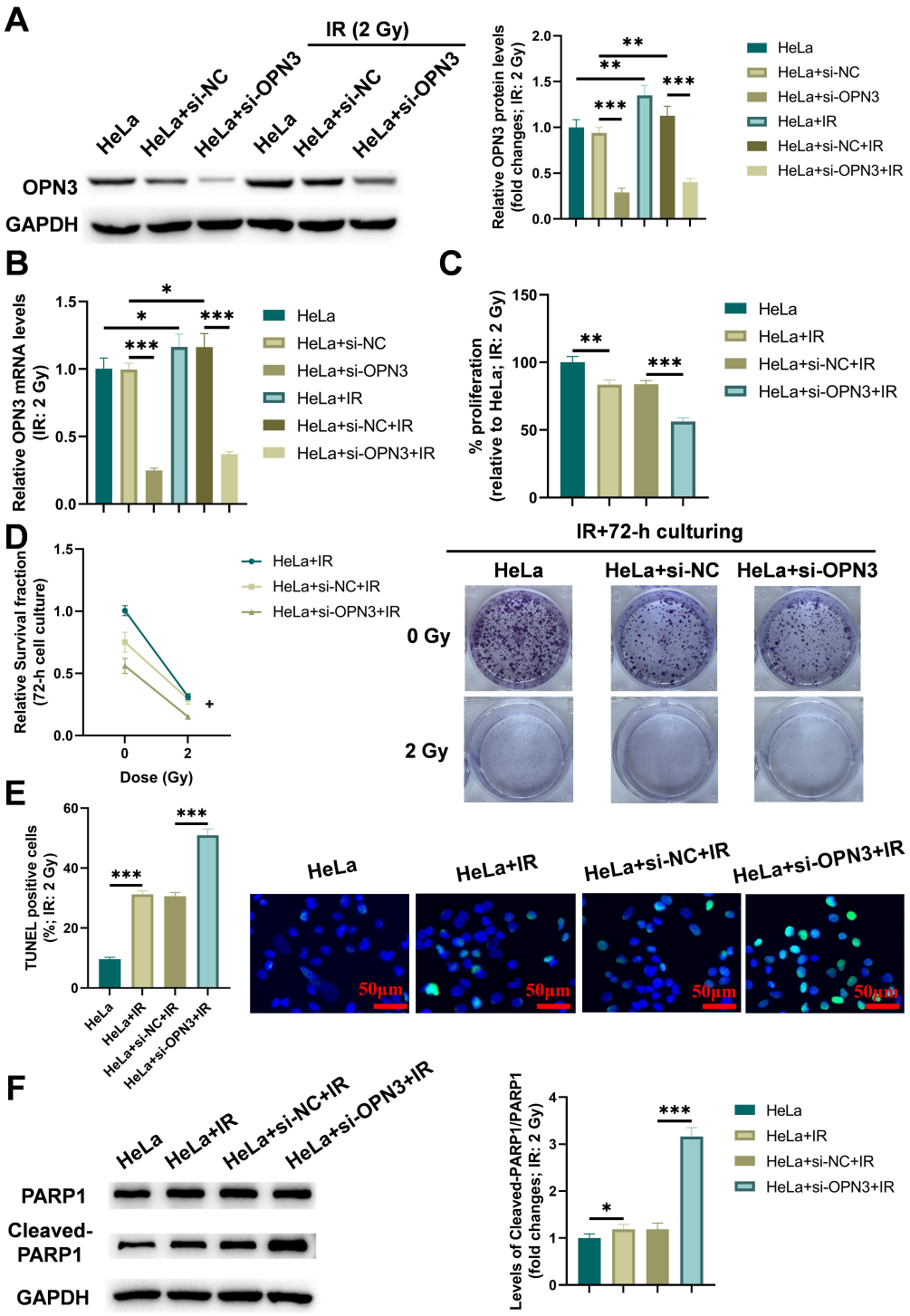

Fig. 1. *OPN3* knockdown enhances radiosensitivity in HeLa cells. (A) Western blot analysis of OPN3 protein levels. (B) Quantification of *OPN3* mRNA levels in differently treated HeLa cells. (C) Cell proliferation assessed by cell counting kit-8 (CCK-8) assay following IR exposure. (D) Survival fraction of cells determined by colony-forming assay after IR exposure. (E) Cell apoptosis detected by TUNEL assay after IR exposure (Scale bar: 50 μm). (F) Levels of Cleaved-PARP1/PARP1 in cells following IR exposure. n = 5. Abbreviations: *OPN3*, opsin 3; *GAPDH*, glyceraldehyde-3-phosphate dehydrogenase; IR, ionizing radiation; TUNEL, terminal deoxynucleotidyl transferase (TdT) dUTP nick-end labeling; PARP1, poly (ADP-ribose) polymerase 1; si-*OPN3*, small interfering RNA (siRNA) targeting *OPN3*; si-NC, negative control scramble siRNA; HeLa+si-NC, si-NC transfected HeLa cells; HeLa+si-*OPN3*, si-*OPN3* transfected HeLa cells; HeLa+IR, HeLa cells treated with IR; HeLa+si-*OPN3*+IR, si-*OPN3* transfected HeLa cells treated with IR; HeLa+si-NC+IR, si-NC transfected HeLa cells treated with IR. n = 6. $^{+}p < 0.05$ HeLa+si-*OPN3*+IR vs. HeLa+si-NC+IR. $^{*}p < 0.05$, $^{**}p < 0.01$, $^{***}p < 0.001$.

Journal of
BIOLOGICAL REGULATORS
and Homeostatic Agents

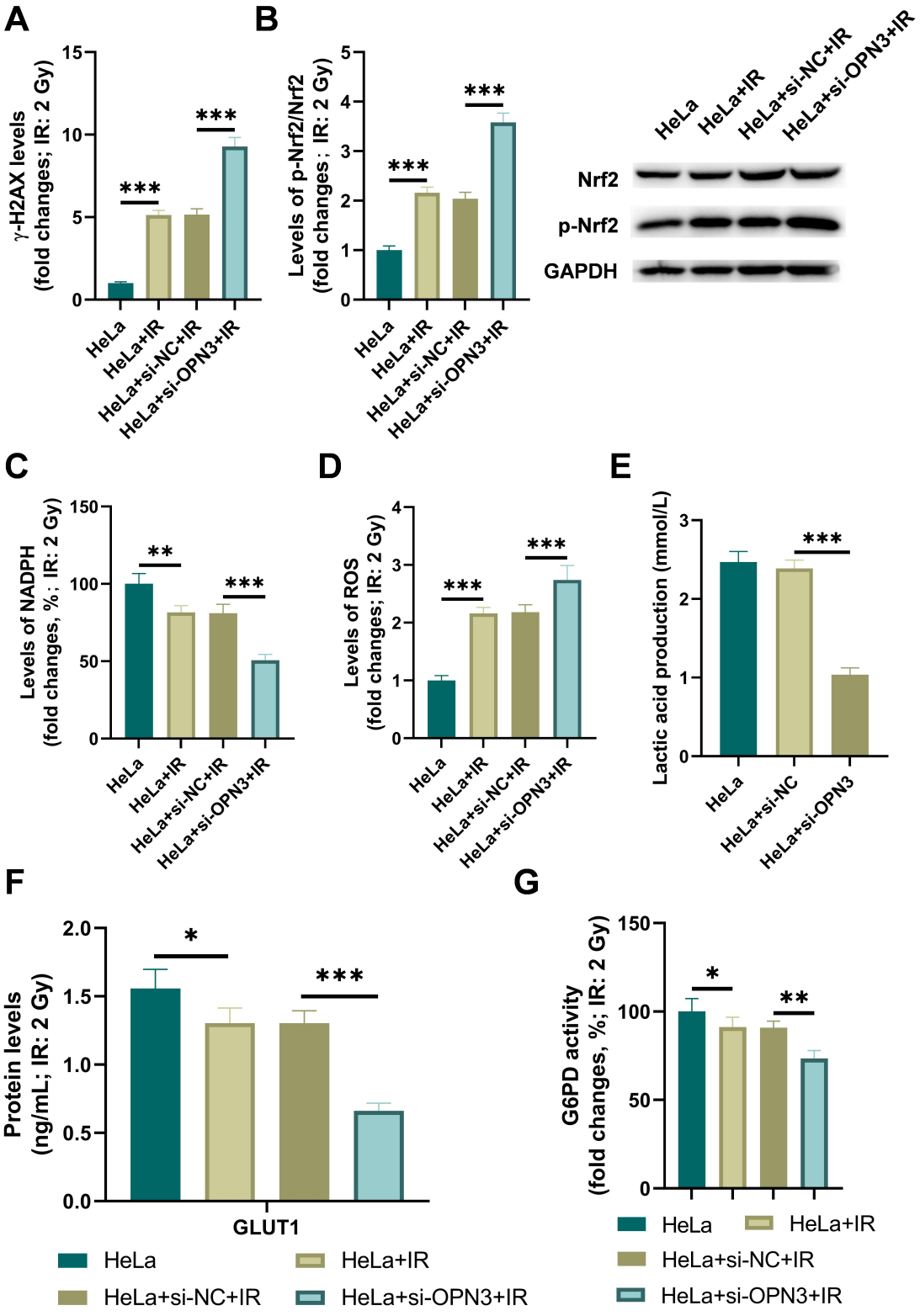

Fig. 2. ***OPN3*** **knockdown increases IR-induced DNA damage and oxidative stress, and suppresses G6PD-mediated glucose metabolism.** (A) Protein levels of γ-H2AX measured by enzyme-linked immunosorbent assay (ELISA). (B) Western blot analysis of phosphorylated (p)-Nrf2/Nrf2 levels. Levels of (C) NADPH, (D) reactive oxygen species (ROS), (E) lactic acid production, (F) GLUT1, and (G) the G6PD activity in differently treated HeLa cells measured by ELISA. n = 5. Abbreviations: γ-H2AX, gamma histone 2AX; NADPH, dihydronicotinamide adenine dinucleotide phosphate; Nrf2, nuclear factor erythroid 2-related factor 2; GLUT1, glucose transporter type 1; G6PD, glucose-6-phosphate dehydrogenase. n = 6. *$p < 0.05$, **$p < 0.01$, ***$p < 0.001$.

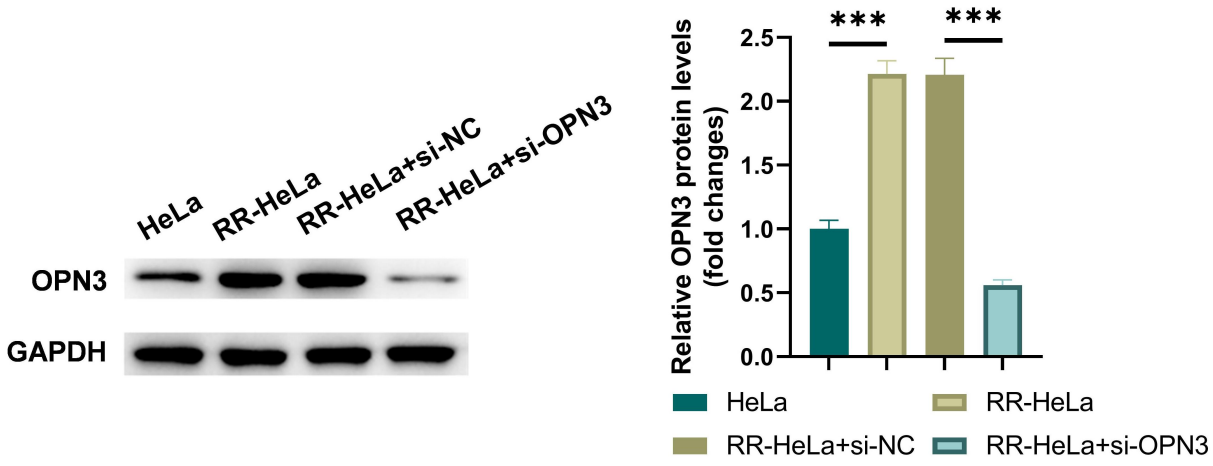

Fig. 3. Establishment of acquired radioresistant HeLa cells with different *OPN3* expression levels. *OPN3* protein levels in differently treated HeLa cells (n = 5). Abbreviations: RR-HeLa, radioresistant HeLa cells; RR-HeLa+si-NC, RR-HeLa cells transfected with si-NC; RR-HeLa+si-*OPN3*, RR-HeLa cells transfected with si-*OPN3*. n = 6. ***$p < 0.001$.

transfected with si-NC (RR-HeLa+si-NC cells) ($p < 0.001$), indicating successful *OPN3* knockdown in RR-HeLa cells through si-*OPN3* transfection.

Validation of Establishment of Radioresistant HeLa Cells and Reversal of Acquired Radioresistance by OPN3 Knockdown in HeLa Cells

The IR treatment (4 Gy) induced fewer TUNEL-positive RR-HeLa cells compared to TUNEL-positive HeLa cells (Fig. 4A; $p < 0.001$) and decreased level of cleaved-PARP1/PARP1 in RR-HeLa cells compared to HeLa cells (Fig. 4B; $p < 0.001$), demonstrating reduced apoptosis of RR-HeLa cells induced by IR. Moreover, after treatment with IR, RR-HeLa cells exhibited higher levels of cell proliferation (Fig. 4C; $p < 0.001$) and survival fraction (Fig. 4D; $p < 0.001$) compared to HeLa cells, indicating increased survivability of RR-HeLa cells under IR. These findings validate the established acquired radioresistance in the RR-HeLa cells. However, IR induced increased TUNEL-positive cells (Fig. 4A; $p < 0.001$) and an increased level of cleaved-PARP1/PARP1 (Fig. 4B; $p < 0.001$) in RR-HeLa+si-*OPN3* cells compared to RR-HeLa+si-NC cells, demonstrating that IR could induce more apoptosis in *OPN3*-knockdown RR-HeLa cells. Furthermore, under IR treatment, cell proliferation (Fig. 4C; $p < 0.001$) and cell survival (Fig. 4D,E; $p < 0.001$) of *OPN3*-knockdown RR-HeLa cells were decreased compared to RR-HeLa+si-NC cells, indicating that *OPN3*-knockdown RR-HeLa cells were less radioresistant. These findings suggest that *OPN3* knockdown disrupts the acquired radioresistance in RR-HeLa cells.

More DNA Damage and Oxidative Stress were Induced by IR in RR-HeLa Cells with OPN3 Knockdown

After IR treatment, the γ-H2AX level was lower in RR-HeLa compared to HeLa cells (Fig. 5A; $p < 0.001$), indicating less DNA damage in RR-HeLa cells. However, compared to RR-HeLa+si-NC cells, IR induced more γ-H2AX in RR-HeLa+si-*OPN3* cells ($p < 0.001$), suggesting that DNA damage was more severe in *OPN3*-knockdown RR-HeLa cells. Moreover, the level of p-Nrf2/Nrf2 was lower in RR-HeLa cells than in HeLa cells after IR treatment (Fig. 5B; $p < 0.001$), and IR triggered an increased level in RR-HeLa+si-*OPN3* cells compared to HeLa+si-NC cells ($p < 0.001$). Additionally, under IR treatment, RR-HeLa cells exhibited a higher level of NADPH (Fig. 5C; $p < 0.001$) and a lower level of ROS (Fig. 5D; $p < 0.001$) compared to HeLa cells. However, compared to RR-HeLa+si-NC cells treated with IR, IR-treated RR-HeLa+si-*OPN3* cells had a lower level of NADPH ($p < 0.001$) and a higher level of ROS ($p < 0.001$). These findings indicate that IR triggers less DNA damage and oxidative stress in RR-HeLa cells, while the self-protection of RR-HeLa against IR was disrupted by *OPN3* knockdown.

OPN3 Knockdown Attenuates G6PD-Mediated Glucose Metabolism in RR-HeLa Cells

As shown in Fig. 5E, a significantly higher lactic acid production in RR-HeLa cells was observed compared to HeLa cells ($p < 0.001$), while si-*OPN3* transfected RR-HeLa cells exhibited significantly lower lactic acid production compared to si-NC transfected RR-HeLa cells ($p < 0.001$). Additionally, exposure to IR increased GLUT1 levels in RR-HeLa cells (Fig. 5F; $p < 0.001$), a response attenuated by *OPN3* knockdown (Fig. 5F; $p < 0.001$).

Journal of
BIOLOGICAL REGULATORS
and Homeostatic Agents

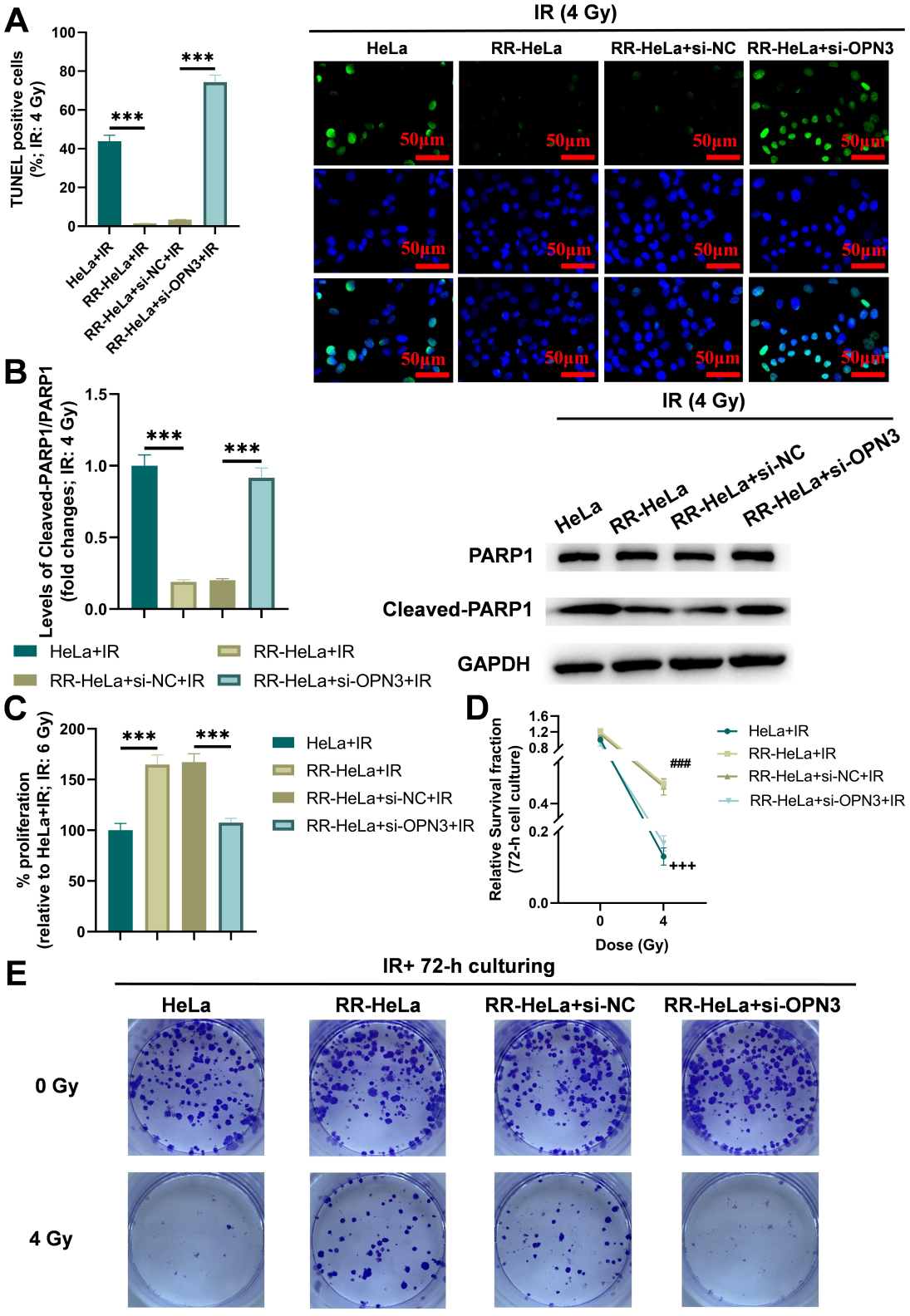

Fig. 4. Validation of acquired radioresistance in HeLa cells and its reversal by *OPN3* knockdown. Cell apoptosis was assessed by (A) TUNEL assay (Scale bar: 50 μm) and (B) levels of cleaved-PARP1/PARP1. (C) Results of CCK-8 assays. (D,E) Survival fraction of cells determined by colony-forming assays. n = 5. Abbreviations: RR-HeLa+IR, RR-HeLa cells treated with IR; RR-HeLa+si-*OPN3*+IR, si-*OPN3* transfected RR-HeLa cells treated with IR; RR-HeLa+si-NC+IR, si-NC transfected RR-HeLa cells treated with IR. n = 6. ***$p < 0.001$. $^{+++}p < 0.001$ HeLa+IR vs RR-HeLa+IR, $^{\#\#\#}p < 0.001$ RR-HeLa+si-NC+IR vs RR-HeLa+si-*OPN3*+IR.

These findings indicate enhanced glucose metabolism upon acquiring radioresistance in HeLa cells, which was mitigated by *OPN3* knockdown. Moreover, the G6PD activity (Fig. 5G; $p < 0.001$) was significantly elevated in RR-HeLa cells following IR treatment compared to HeLa cells, while this elevation was decreased by *OPN3* knockdown (Fig. 5G; $p < 0.001$). These findings suggest a correlation between enhanced glucose metabolism mediated by G6PD and radioresistance in RR-HeLa cells, which can be suppressed by *OPN3* knockdown, compromising radioresistance in RR-HeLa cells.

OPN3 Knockdown Reverses Radioresistance in HeLa Cells by Elevating Oxidative Stress and Reducing G6PD Levels

To further validate the impact of *OPN3* on radioresistance, we investigated the effect of increased *OPN3* levels on the HeLa cell proliferation under IR. Fig. 6A demonstrates the successful elevation of *OPN3* protein levels in OE-*OPN3* transfected HeLa cells ($p < 0.001$). As shown in Fig. 6B, cell proliferation decreased in HeLa cells under IR ($p < 0.01$). However, compared to OE-NC-transfected HeLa cells, HeLa transfected with OE-*OPN3* proliferated more under IR ($p < 0.05$), suggesting that elevated OPN3 levels promoted radioresistance in HeLa cells. These observations, combined with the earlier findings, strongly support the role of *OPN3* in enhancing the radioresistance, while *OPN3* knockdown sensitized HeLa cells to radiation.

As shown previously, *OPN3* knockdown increased the ROS levels in HeLa and RR-HeLa cells. We employed the N-acetylcysteine (NAC), a ROS scavenger, to investigate the role of ROS in *OPN3* knockdown-mediated sensitization to radiation. Cell proliferation of HeLa cells decreased under IR (Fig. 6C; $p < 0.01$), further reduced by *OPN3* knockdown ($p < 0.001$), and reversed by NAC ($p < 0.001$). These findings suggest that *OPN3* knockdown attenuated radioresistance by enhancing ROS levels in HeLa cells. This suggestion is supported by results in Fig. 6D, showing increased proliferation of RR-HeLa cells compared to HeLa cells under IR ($p < 0.001$). *OPN3* knockdown decreased this proliferative capacity ($p < 0.001$), which was restored by NAC ($p < 0.001$), indicating that *OPN3* knockdown suppressed radioresistance in RR-HeLa cells by increasing ROS levels and oxidative stress.

Further "loss and gain" experiments were conducted to verify the role of G6PD levels in *OPN3* knockdown-mediated reversal of radioresistance. Fig. 6E illustrates that *OPN3* knockdown decreased HeLa cell proliferation under IR ($p < 0.001$), which was further reduced by 6-aminonicotinamide (6-AN), a specific G6PD inhibitor ($p < 0.01$). Similarly, as shown in Fig. 6F, *OPN3* knockdown reversed radioresistance in RR-HeLa cells, resulting in reduced proliferation ($p < 0.001$), and the 6-AN further diminished more of the radioresistance, resulting in reduced proliferation ($p < 0.01$). These findings indicate a direct association between G6PD suppression and reversal of radioresistance.

Moreover, we overexpressed G6PD in *OPN3*-knockdown HeLa cells to investigate whether *OPN3* knockdown sensitized cells to radiation by reducing G6PD levels. Fig. 6G confirms decreased G6PD levels in *OPN3* knockdown HeLa cells compared to si-NC transfected cells ($p < 0.001$) and subsequent increase after transfection with OE-G6PD ($p < 0.001$), indicating successful transfection and upregulation of G6PD expression. Consequently, Fig. 6H shows that *OPN3* knockdown sensitized HeLa cells to radiation, resulting in reduced proliferation ($p < 0.001$), while additional G6PD expression in *OPN3* knockdown HeLa cells reversed this effect, leading to increased proliferation under IR ($p < 0.001$). These findings demonstrate that *OPN3* knockdown could not overcome radioresistance when G6PD levels were not successfully decreased, highlighting the pivotal role of G6PD downregulation in reversing radioresistance by *OPN3* knockdown.

OPN3 Knockdown Reduces G6PD Levels by Promoting G6PD Degradation Mediated by the Autophagy-Lysosome Pathway

We further explored the mechanisms underlying *OPN3*-mediated G6PD degradation, focusing on the proteasomal and autophagic lysosomal pathways responsible for protein degradation. As shown in Fig. 7A, G6PD levels decreased upon *OPN3* knockdown in RR-HeLa cells ($p < 0.001$). Notably, this reduction in G6PD was reversed by the autophagy inhibitor chloroquine (an autophagy inhibitor) (CQ) ($p < 0.001$), while the proteasome pathway inhibitor MG132 did not elicit any significant change ($p > 0.05$). Moreover, the CQ-induced increase in G6PD levels remained unchanged by MG132 ($p > 0.05$). These findings suggest that *OPN3* knockdown reduces G6PD levels by promoting autophagic lysosomal pathway-mediated G6PD degradation.

To verify these findings, we conducted western blot analysis to assess autophagy-related protein levels under IR treatment. As illustrated in Fig. 7B,C, *OPN3* knockdown in RR-HeLa cells led to decreased G6PD levels and increased LC3B II levels ($p < 0.01$ and $p < 0.001$, respectively), corresponding to reduced cell proliferation (Fig. 7D; $p < 0.001$) under IR treatment. Notably, these alterations were reversed by the autophagy inhibitor CQ (G6PD, $p < 0.001$; LC3B II, $p < 0.001$; cell proliferation, $p < 0.001$). Collectively, these findings demonstrate that *OPN3* knockdown overcomes radioresistance by promoting autophagic degradation of G6PD, leading to reduced G6PD levels.

Journal of
BIOLOGICAL REGULATORS
and Homeostatic Agents

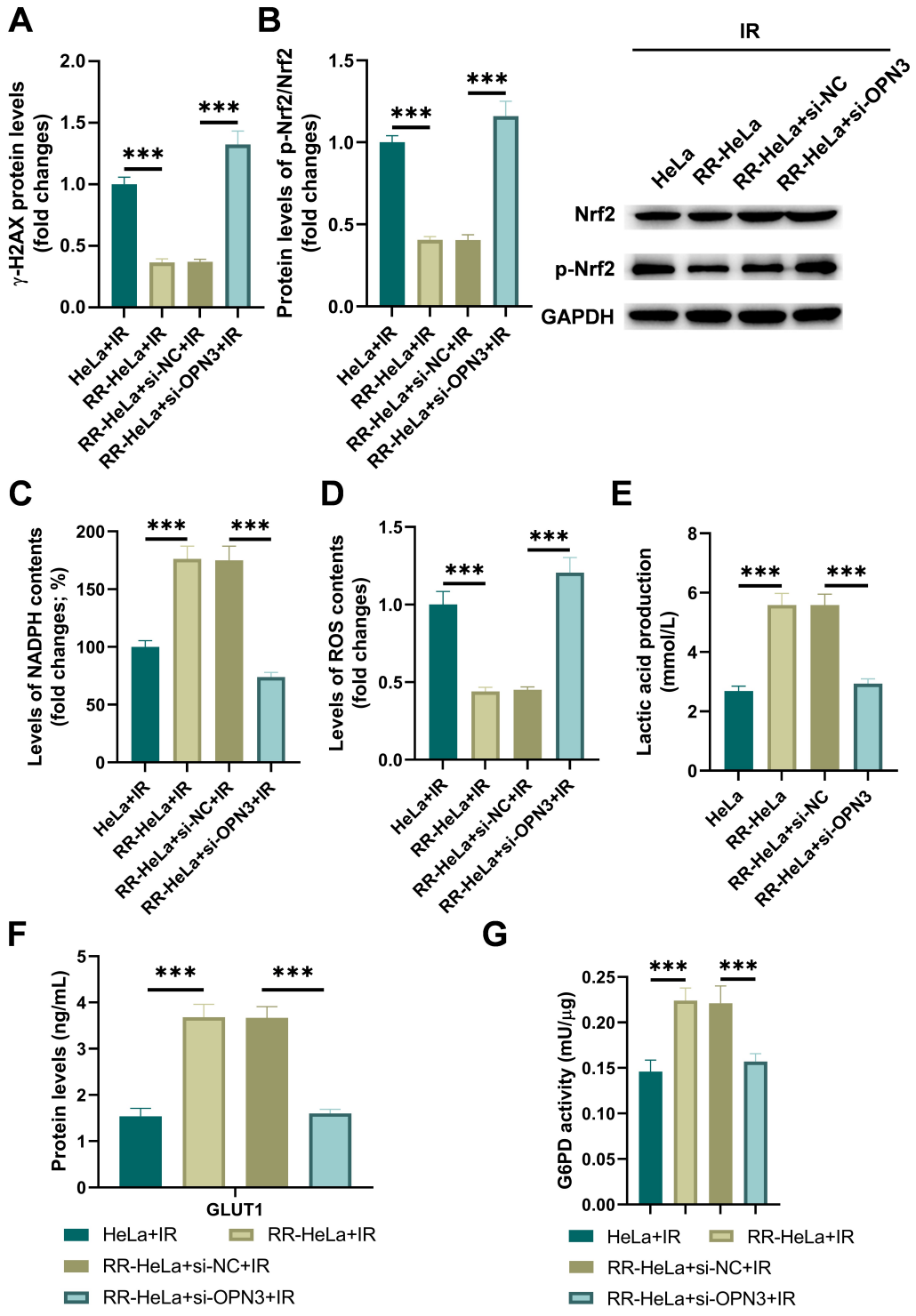

Fig. 5. *OPN3* knockdown disrupts the self-protection mechanisms of RR-HeLa cells against DNA damage and oxidative stress, and suppresses G6PD-mediated glucose metabolism. (A) Protein levels of γ-H2AX detected by ELISA. (B) Western blot analysis of phosphorylated Nrf2 (p-Nrf2)/Nrf2 levels. Levels of (C) NADPH and (D) ROS. (E) Lactic acid production. (F) Protein levels of GLUT1. (G) G6PD activity. n = 6. ***$p < 0.001$.

Discussion

This study firstly provides novel insights into the role of *OPN3*, primarily its knockdown, in cervical cancer (CC) therapeutic resistance and highlights the association between *OPN3* knockdown and the G6PD-mediated pentose phosphate (PPP) underlying CC radioresistance. Our results indicate that *OPN3* may contribute to the develop-

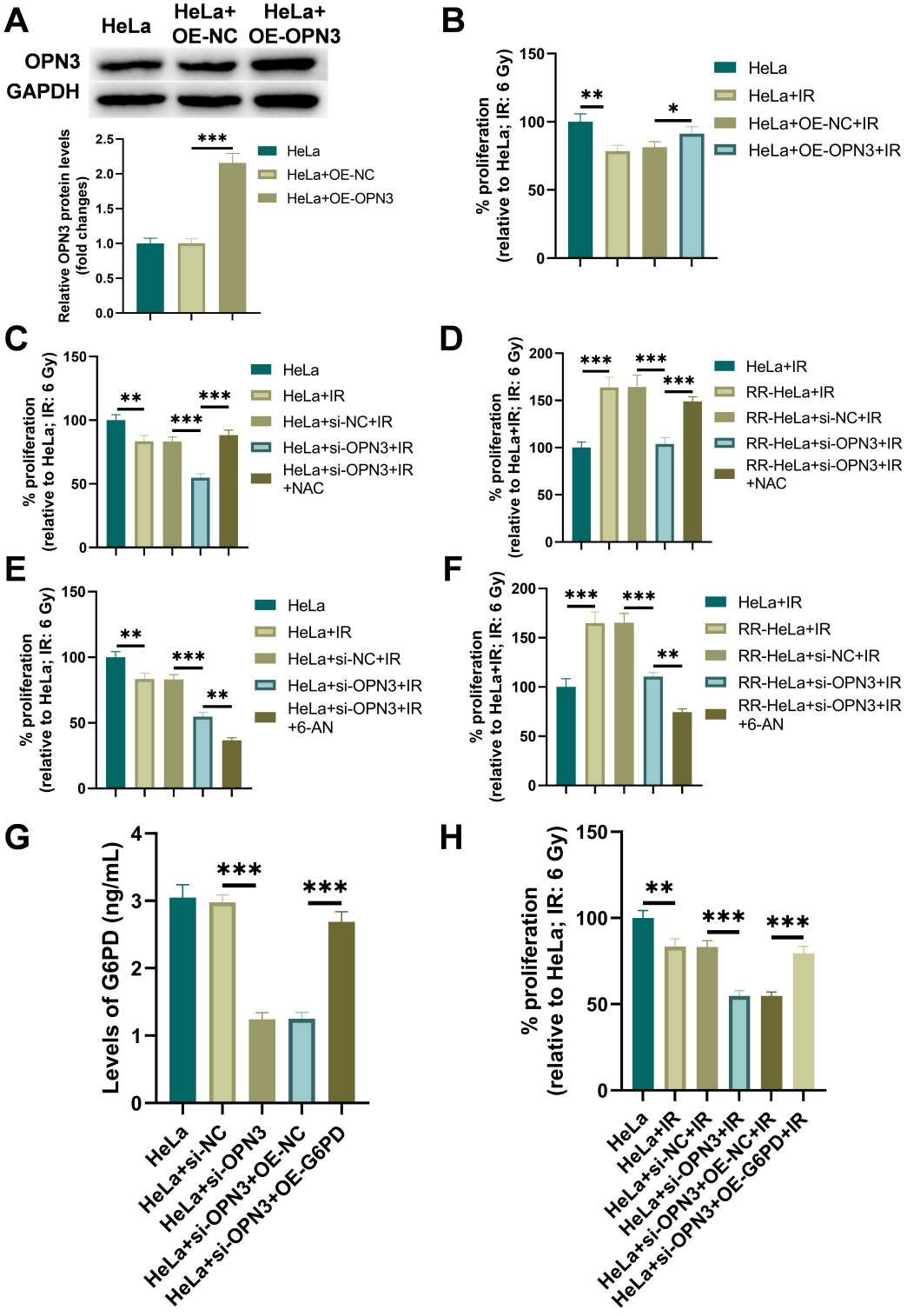

Fig. 6. *OPN3* knockdown overcomes radioresistance in HeLa cells by increasing oxidative stress and reducing G6PD levels. (A) OPN3 protein levels in transfected HeLa cells. (B) Cell proliferation assessed by CCK-8 assay measuring the effect of increased OPN3 protein level on proliferation of HeLa cells. Effects of N-acetylcysteine (NAC; the ROS scavenger) on proliferation of (C) HeLa cells and (D) RR-HeLa cells assessed by CCK-8 assays. Effect of 6-aminonicotinamide (6-AN; the specific inhibitor of G6PD) on proliferation of (E) HeLa cells and (F) RR-HeLa cells assessed by CCK-8 assays. Levels of (G) G6PD protein and (H) corresponding cell proliferation in differently treated HeLa cells. Abbreviations: OE-NC, empty vector; OE-G6PD, G6PD-overexpressing plasmids. n = 6. *$p < 0.05$, **$p < 0.01$, ***$p < 0.001$.

Journal of
BIOLOGICAL REGULATORS
and Homeostatic Agents

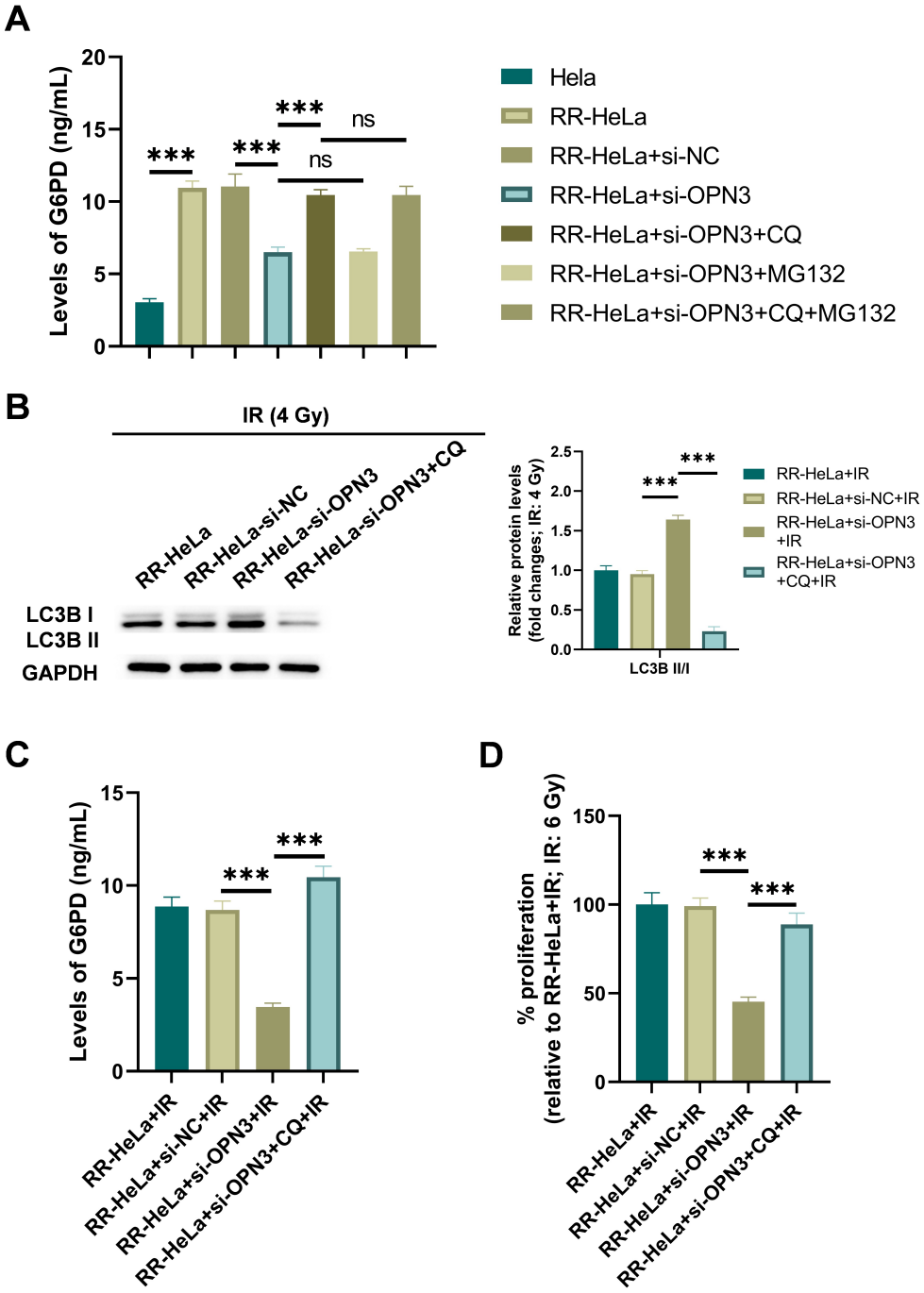

Fig. 7. *OPN3* knockdown reduces G6PD levels by promoting the G6PD degradation mediated by the autophagy-lysosome pathway. (A) Protein levels of G6PD detected by ELISA. (B) Western blot analysis of LC3B II levels. (C) G6PD protein levels detected by ELISA. (D) Cell proliferation assessed by CCK-8 assay. n = 6. Abbreviations: CQ, chloroquine (an autophagy inhibitor); LC3B, light chain 3B. ***$p < 0.001$; ns, no significance ($p > 0.05$).

ment of radioresistance in CC cells, and its inhibition may enhance DNA damage and oxidative stress by suppressing G6PD expression and activity, thereby promoting cell apoptosis upon ionization radiation (IR) treatment. Additionally, the capacity of *OPN3* knockdown to overcome radioresistance in CC cells was associated with the acceleration of G6PD degradation through the autophagy process.

OPN3, crucial in light-dependent and light-independent processes, has been identified as a risk factor for various cancers [18–20,30]. Notably, a previous

study demonstrated that downregulation of *OPN3* induces melanocyte apoptosis through the mitochondrial apoptosis pathway [31], implicating *OPN3* in mitochondrial function and dysfunction. Oxidative stress has been shown to induce mitochondrial dysfunction [32], and glucose levels and metabolism influence mitochondrial dysfunction [33]. In this study, we observed that *OPN3* knockdown increased apoptosis in CC cells following IR treatment, accompanied by elevated oxidative stress and DNA damage, and decreased glucose metabolism. These findings suggest that *OPN3* knockdown increases the sensitivity of HeLa cells to IR by enhancing oxidative stress and DNA damage while reducing glucose metabolism. However, further investigation is needed to determine whether these effects result in mitochondrial dysfunction in CC cells.

Radiotherapy (RT) is a critical and pivotal component in treating CC, especially in advanced stages [34]. The efficacy of RT lies in its ability to induce various mechanisms for tumor cell eradication. Ionizing radiation penetrates tissues, disrupting chemical bonds, causing electron removal from atoms, and inducing chromosomal mutations, notably by forming DNA double-strand breaks (DSBs), which represent a pivotal mechanism for cell death [35–37].

Moreover, RT triggers the generation of ROS, indirectly contributing to cancer cell death through various biological alterations, apoptosis, autophagy, and necrotic cell death pathways [38,39]. Photodynamic therapy, a widely used clinical approach, is based on inducing ROS to eliminate CC cells [40]. Our study demonstrates that *OPN3* knockdown augments radiosensitivity or disrupts radioresistance in CC cells by enhancing IR-induced DNA damage and ROS production in HeLa cells. These observations align with the notion that increased DNA damage and ROS levels promote cancer cell death, underscoring the potential efficacy of OPN3 knockdown in radiosensitizing CC cells.

Another strategy to enhance radiosensitivity in CC involves inhibiting DNA repair mechanisms [34]. Two critical pathways, homologous recombination (HR) and non-homologous end joining (NHEJ), participate in DNA repair post-RT [41]. Previous studies have shown that inhibiting HR- and NHEJ-related genes heightens cancer cell sensitivity to RT [42,43]. PARP1, a key sensor of DNA damage, is crucial in repairing single-strand DNA breaks. However, cleavage of PARP1 leads to its inactivation, thereby suppressing DNA repair processes [44]. Inhibition of PARP1 has been demonstrated to enhance radiosensitivity in CC [45,46]. Our findings reveal that *OPN3* knockdown increases DNA damage, as evidenced by elevated levels of γ-H2AX, while concurrently suppressing DNA repair, indicated by increased levels of cleaved-PARP1 in CC cells. This further underscores the relationship between heightened DNA damage and suppressed DNA repair in promoting radiosensitivity, thus elucidating how *OPN3* knockdown promotes radiosensitivity in CC cells.

Furthermore, glucose metabolism is critical in CC progression, as the growth and proliferation of CC cells primarily rely on energy obtained through aerobic glycolysis, making glycolysis inhibition a promising therapeutic strategy for CC treatment [47]. GLUT1, a key enzyme in CC cells, facilitates aerobic glycolysis by promoting glucose uptake and lactate production, thus promoting CC progression [48,49]. Upregulation of GLUTs is a common feature of cancer cells to meet their high energy demand [50]. In our study, we observed that *OPN3* knockdown decreased GLUT1 levels, suppressing aerobic glycolysis, and consequently, CC cell proliferation.

Additionally, glycolysis generates metabolic intermediates and precursors that enter various biosynthetic pathways, including the PPP, to generate amino acids and nucleic acids required for synthesizing biological macromolecules and organelles, such as lactic acid and NADPH, necessary for cell proliferation [51]. The rate of metabolic intermediates fluxing into PPP is regulated by G6PD [23], and products generated during this process enhance the antioxidant capacity of cells, conferring resistance to RT [52]. However, in our study, we observed that *OPN3* knockdown decreased G6PD levels, as well as levels of lactic acid and NADPH, conversely sensitized CC cells to RT.

Our study demonstrates that *OPN3* knockdown radiosensitizes CC HeLa cells by suppressing G6PD-meditaed glucose metabolism, DNA repair, lactic acid and NADPH production, while increasing oxidative stress and DNA damage, all of which have been previously associated with CC radioresistance. However, further validation of these findings is warranted using additional CC cell lines, and animal studies are critical for future clinical applications.

Conclusion

The findings of this study highlight the role of *OPN3* knockdown in radiosensitizing HeLa cells and overcoming radioresistance. By promoting the autophagic degradation of G6PD and exacerbating oxidative stress, *OPN3* knockdown enhances the radiosensitivity of HeLa cells. These findings contribute to a deeper understanding of CC cell radioresistance mechanisms and underscore the potential of *OPN3* knockdown as an effective therapeutic strategy for enhancing the radiosensitivity of CC cells. Ultimately, these findings may hold promise for improving the efficiency of clinical radiotherapy in the treatment of CC.

Availability of Data and Materials

Data to support the findings of this study are available on reasonable request from the corresponding author.

Journal of
BIOLOGICAL REGULATORS
and Homeostatic Agents

Author Contributions

YL performed the research. YL and XW provided help and advice on the experiments. XW contributed to the analysis and interpretation of the data. Both authors contributed to editorial changes in the manuscript. Both authors read and approved the final manuscript. Both authors have participated sufficiently in the work to take public responsibility for appropriate portions of the content and agreed to be accountable for all aspects of the work in ensuring that questions related to its accuracy or integrity.

Ethics Approval and Consent to Participate

Not applicable.

Acknowledgment

Not applicable.

Funding

This research received no external funding.

Conflict of Interest

The authors declare no conflict of interest.

References

[1] Sung H, Ferlay J, Siegel RL, Laversanne M, Soerjomataram I, Jemal A, *et al*. Global Cancer Statistics 2020: GLOBOCAN Estimates of Incidence and Mortality Worldwide for 36 Cancers in 185 Countries. CA: a Cancer Journal for Clinicians. 2021; 71: 209–249.

[2] Fernandes A, Viveros-Carreño D, Hoegl J, Ávila M, Pareja R. Human papillomavirus-independent cervical cancer. International Journal of Gynecological Cancer: Official Journal of the International Gynecological Cancer Society. 2022; 32: 1–7.

[3] Hemmat N, Bannazadeh Baghi H. Association of human papillomavirus infection and inflammation in cervical cancer. Pathogens and Disease. 2019; 77: ftz048.

[4] Hu K, Wang W, Liu X, Meng Q, Zhang F. Comparison of treatment outcomes between squamous cell carcinoma and adenocarcinoma of cervix after definitive radiotherapy or concurrent chemoradiotherapy. Radiation Oncology (London, England). 2018; 13: 249.

[5] Williams J, Kostiuk M, Biron VL. Molecular Detection Methods in HPV-Related Cancers. Frontiers in Oncology. 2022; 12: 864820.

[6] Kombe Kombe AJ, Li B, Zahid A, Mengist HM, Bounda GA, Zhou Y, *et al*. Epidemiology and Burden of Human Papillomavirus and Related Diseases, Molecular Pathogenesis, and Vaccine Evaluation. Frontiers in Public Health. 2021; 8: 552028.

[7] Rotondo JC, Oton-Gonzalez L, Mazziotta C, Lanzillotti C, Iaquinta MR, Tognon M, *et al*. Simultaneous Detection and Viral DNA Load Quantification of Different Human Papillomavirus Types in Clinical Specimens by the High Analytical Droplet Digital PCR Method. Frontiers in Microbiology. 2020; 11: 591452.

[8] Perkins RB, Wentzensen N, Guido RS, Schiffman M. Cervical Cancer Screening: A Review. JAMA. 2023; 330: 547–558.

[9] Arbyn M, Weiderpass E, Bruni L, de Sanjosé S, Saraiya M, Ferlay J, *et al*. Estimates of incidence and mortality of cervical cancer in 2018: a worldwide analysis. The Lancet. Global Health. 2020; 8: e191–e203.

[10] Mayadev JS, Ke G, Mahantshetty U, Pereira MD, Tarnawski R, Toita T. Global challenges of radiotherapy for the treatment of locally advanced cervical cancer. International Journal of Gynecological Cancer: Official Journal of the International Gynecological Cancer Society. 2022; 32: 436–445.

[11] Bhatla N, Aoki D, Sharma DN, Sankaranarayanan R. Cancer of the cervix uteri. International Journal of Gynaecology and Obstetrics: the Official Organ of the International Federation of Gynaecology and Obstetrics. 2018; 143: 22–36.

[12] DeBoer RJ, Umutoni V, Bazzett-Matabele L, Katznelson E, Nguyen C, Umwizerwa A, *et al*. Cervical cancer treatment in Rwanda: Resource-driven adaptations, quality indicators, and patient outcomes. Gynecologic Oncology. 2022; 164: 370–378.

[13] Nin DS, Wujanto C, Tan TZ, Lim D, Damen JMA, Wu KY, *et al*. GAGE mediates radio resistance in cervical cancers via the regulation of chromatin accessibility. Cell Reports. 2021; 36: 109621.

[14] Zeng X, Wan L, Wang Y, Xue J, Yang H, Zhu Y. Effect of low dose of berberine on the radioresistance of cervical cancer cells via a PI3K/HIF-1 pathway under nutrient-deprived conditions. International Journal of Radiation Biology. 2020; 96: 1060–1067.

[15] Huang RX, Zhou PK. DNA damage response signaling pathways and targets for radiotherapy sensitization in cancer. Signal Transduction and Targeted Therapy. 2020; 5: 60.

[16] Feng Y, Wang Z, Yang N, Liu S, Yan J, Song J, *et al*. Identification of Biomarkers for Cervical Cancer Radiotherapy Resistance Based on RNA Sequencing Data. Frontiers in Cell and Developmental Biology. 2021; 9: 724172.

[17] Jiao X, Zhang S, Jiao J, Zhang T, Qu W, Muloye GM, *et al*. Promoter methylation of SEPT9 as a potential biomarker for early detection of cervical cancer and its overexpression predicts radioresistance. Clinical Epigenetics. 2019; 11: 120.

[18] Zeng W, Zhang W, Feng J, He X, Lu H. Expression of OPN3 in acral lentiginous melanoma and its associated with clinicohistopathologic features and prognosis. Immunity, Inflammation and Disease. 2021; 9: 840–850.

[19] Xu C, Wang R, Yang Y, Xu T, Li Y, Xu J, *et al*. Expression of OPN3 in lung adenocarcinoma promotes epithelial-mesenchymal transition and tumor metastasis. Thoracic Cancer. 2020; 11: 286–294.

[20] Miyanaga A, Masuda M, Motoi N, Tsuta K, Nakamura Y, Nishijima N, *et al*. Whole-exome and RNA sequencing of pulmonary carcinoid reveals chromosomal rearrangements associated with recurrence. Lung Cancer (Amsterdam, Netherlands). 2020; 145: 85–94.

[21] Bian C, Zheng Z, Su J, Wang H, Chang S, Xin Y, *et al*. Targeting Mitochondrial Metabolism to Reverse Radioresistance: An Alternative to Glucose Metabolism. Antioxidants (Basel, Switzerland). 2022; 11: 2202.

[22] Mittal A, Nenwani M, Sarangi I, Achreja A, Lawrence TS, Nagrath D. Radiotherapy-induced metabolic hallmarks in the tumor microenvironment. Trends in Cancer. 2022; 8: 855–869.

[23] Deng H, Chen Y, Wang L, Zhang Y, Hang Q, Li P, *et al*. PI3K/mTOR inhibitors promote G6PD autophagic degradation and exacerbate oxidative stress damage to radiosensitize small cell lung cancer. Cell Death & Disease. 2023; 14: 652.

[24] Li Z, Zhang Y, Sui S, Hua Y, Zhao A, Tian X, *et al*. Targeting HMGB3/hTERT axis for radioresistance in cervical cancer. Journal of Experimental & Clinical Cancer Research: CR. 2020; 39: 243.

[25] Halasi M, Wang M, Chavan TS, Gaponenko V, Hay N, Gartel

AL. ROS inhibitor N-acetyl-L-cysteine antagonizes the activity of proteasome inhibitors. The Biochemical Journal. 2013; 454: 201–208.

[26] Cheng J, Huang Y, Zhang X, Yu Y, Wu S, Jiao J, *et al*. TRIM21 and PHLDA3 negatively regulate the crosstalk between the PI3K/AKT pathway and PPP metabolism. Nature Communications. 2020; 11: 1880.

[27] Said A, Bock S, Lajqi T, Müller G, Weindl G. Chloroquine promotes IL-17 production by CD4+ T cells via p38-dependent IL-23 release by monocyte-derived Langerhans-like cells. Journal of Immunology (Baltimore, Md.: 1950). 2014; 193: 6135–6143.

[28] Lee CS, Han ES, Park ES, Bang H. Inhibition of MG132-induced mitochondrial dysfunction and cell death in PC12 cells by 3-morpholinosydnonimine. Brain Research. 2005; 1036: 18–26.

[29] Delaidelli A, Richner M, Jiang L, van der Laan A, Bergholdt Jul Christiansen I, Ferreira N, *et al*. α-Synuclein pathology in Parkinson disease activates homeostatic NRF2 anti-oxidant response. Acta Neuropathologica Communications. 2021; 9: 105.

[30] Ozdeslik RN, Olinski LE, Trieu MM, Oprian DD, Oancea E. Human nonvisual opsin 3 regulates pigmentation of epidermal melanocytes through functional interaction with melanocortin 1 receptor. Proceedings of the National Academy of Sciences of the United States of America. 2019; 116: 11508–11517.

[31] Wang Y, Lan Y, Lu H. Opsin3 Downregulation Induces Apoptosis of Human Epidermal Melanocytes via Mitochondrial Pathway. Photochemistry and Photobiology. 2020; 96: 83–93.

[32] Kim SH, Kim H. Inhibitory Effect of Astaxanthin on Oxidative Stress-Induced Mitochondrial Dysfunction-A Mini-Review. Nutrients. 2018; 10: 1137.

[33] Ito M, Gurumani MZ, Merscher S, Fornoni A. Glucose- and Non-Glucose-Induced Mitochondrial Dysfunction in Diabetic Kidney Disease. Biomolecules. 2022; 12: 351.

[34] Ni M, Li J, Zhao H, Xu F, Cheng J, Yu M, *et al*. BRD4 inhibition sensitizes cervical cancer to radiotherapy by attenuating DNA repair. Oncogene. 2021; 40: 2711–2724.

[35] Kuwahara Y, Tomita K, Roudkenar MH, Roushandeh AM, Urushihara Y, Igarashi K, *et al*. The Effects of Hydrogen Peroxide and/or Radiation on the Survival of Clinically Relevant Radioresistant Cells. Technology in Cancer Research & Treatment. 2020; 19: 1533033820980077.

[36] Centurione L, Aiello FB. DNA Repair and Cytokines: TGF-β, IL-6, and Thrombopoietin as Different Biomarkers of Radioresistance. Frontiers in Oncology. 2016; 6: 175.

[37] Zhao Y, Chen S. Targeting DNA Double-Strand Break (DSB) Repair to Counteract Tumor Radio-resistance. Current Drug Targets. 2019; 20: 891–902.

[38] Lee SY, Jeong EK, Ju MK, Jeon HM, Kim MY, Kim CH, *et al*. Induction of metastasis, cancer stem cell phenotype, and oncogenic metabolism in cancer cells by ionizing radiation. Molecular Cancer. 2017; 16: 10.

[39] Zou Z, Chang H, Li H, Wang S. Induction of reactive oxygen species: an emerging approach for cancer therapy. Apoptosis: an International Journal on Programmed Cell Death. 2017; 22: 1321–1335.

[40] Xin Y, Guo W, Yang C, Huang Q, Zhang P, Zhang L, *et al*. Photodynamic Effects of Vitamin K3 on Cervical Carcinoma Cells Activating Mitochondrial Apoptosis Pathways. Anti-cancer Agents in Medicinal Chemistry. 2021; 21: 91–99.

[41] Fu S, Jin L, Gong T, Pan S, Zheng S, Zhang X, *et al*. Effect of sinomenine hydrochloride on radiosensitivity of esophageal squamous cell carcinoma cells. Oncology Reports. 2018; 39: 1601–1608.

[42] Zhang J, Chen M, Pang Y, Cheng M, Huang B, Xu S, *et al*. Flap endonuclease 1 and DNA-PKcs synergistically participate in stabilizing replication fork to encounter replication stress in glioma cells. Journal of Experimental & Clinical Cancer Research: CR. 2022; 41: 140.

[43] Guo Z, Wang YH, Xu H, Yuan CS, Zhou HH, Huang WH, *et al*. LncRNA linc00312 suppresses radiotherapy resistance by targeting DNA-PKcs and impairing DNA damage repair in nasopharyngeal carcinoma. Cell Death & Disease. 2021; 12: 69.

[44] Mashimo M, Onishi M, Uno A, Tanimichi A, Nobeyama A, Mori M, *et al*. The 89-kDa PARP1 cleavage fragment serves as a cytoplasmic PAR carrier to induce AIF-mediated apoptosis. The Journal of Biological Chemistry. 2021; 296: 100046.

[45] Raspaglio G, Buttarelli M, Filippetti F, Battaglia A, Buzzonetti A, Scambia G, *et al*. Stat1 confers sensitivity to radiation in cervical cancer cells by controlling Parp1 levels: a new perspective for Parp1 inhibition. Cell Death & Disease. 2021; 12: 933.

[46] IJff M, van Bochove GGW, Whitton D, Winiarczyk R, Honhoff C, Rodermond H, *et al*. PARP1-Inhibition Sensitizes Cervical Cancer Cell Lines for Chemoradiation and Thermoradiation. Cancers. 2021; 13: 2092.

[47] Liu Z, Zhu W, Kong X, Chen X, Sun X, Zhang W, *et al*. Tanshinone IIA inhibits glucose metabolism leading to apoptosis in cervical cancer. Oncology Reports. 2019; 42: 1893–1903.

[48] Zhang Y, Zhao L, Yang S, Cen Y, Zhu T, Wang L, *et al*. CircCDKN2B-AS1 interacts with IMP3 to stabilize hexokinase 2 mRNA and facilitate cervical squamous cell carcinoma aerobic glycolysis progression. Journal of Experimental & Clinical Cancer Research: CR. 2020; 39: 281.

[49] Ferrer CM, Lynch TP, Sodi VL, Falcone JN, Schwab LP, Peacock DL, *et al*. O-GlcNAcylation regulates cancer metabolism and survival stress signaling via regulation of the HIF-1 pathway. Molecular Cell. 2014; 54: 820–831.

[50] Jiang X, Yuan J, Dou Y, Zeng D, Xiao S. Lipopolysaccharide Affects the Proliferation and Glucose Metabolism of Cervical Cancer Cells Through the FRA1/MDM2/p53 Pathway. International Journal of Medical Sciences. 2021; 18: 1030–1038.

[51] Zhu Y, Qiu Y, Zhang X. TKTL1 participated in malignant progression of cervical cancer cells via regulating AKT signal mediated PFKFB3 and thus regulating glycolysis. Cancer Cell International. 2021; 21: 678.

[52] Hanahan D, Weinberg RA. Hallmarks of cancer: the next generation. Cell. 2011; 144: 646–674.